Available online at www.sciencedirect.com
ScienceDirect
Journal of Sound and Vibration 311 (2008) 1465–1475
JOURNAL OF SOUND AND VIBRATION
www.elsevier.com/locate/jsvi

Short Communication

Modal disparity and its experimental verification

Jimmy Issa, Ranjan Mukherjee*, Alejandro R. Diaz, Steven W. Shaw

Department of Mechanical Engineering, Michigan State University, East Lansing, MI 48824, USA

Received 5 March 2007; received in revised form 2 October 2007; accepted 16 October 2007
Available online 11 December 2007

Abstract

This paper describes an analytical and experimental investigation of the property of modal disparity in a vibrating structure. For a given structure, the concept of modal disparity describes the structure's ability to generate significant changes in the mode shapes by some type of on-the-fly structural modification. In the present study we consider a vibrating beam that experiences a controlled stiffness change, induced by the activation and deactivation of an electromagnetic brake that causes a spatially localized change in the bending stiffness. Using a finite element model and an experimental apparatus it is shown that significant amounts of energy can be shifted back and forth between sets of modes in a systematic and predictable manner. This confirmation of modal disparity for a specific structural system provides evidence that this concept is feasible, and thereby opens the door for a number of potential applications in passive and active control of vibrating structures.

1. Introduction

The controlled redistribution of energy in vibrating structures is at the heart of many engineering problems with important practical applications. Modal control strategies, vibration absorbers, and some forms of energy harvesting, all rely in one form or another on the redistribution of energy in vibrating structures from mode to mode and, in space, from one region of the structure to another. A new methodology for design of structures to achieve a targeted and purposeful redistribution of vibration energy was recently proposed by the authors [1,2]. This methodology relies on *modal disparity*, a quantifiable property of the structure being designed, and relies on a carefully crafted variation in the stiffness of the structure. In this paper we present experimental results that illustrates the presence of modal disparity in a simple structure.

Stiffness variation, by itself, is not a new concept. For example, Clark [3] and Corr and Clark [4] proposed stiffness variation of piezoelectric actuators to accomplish energy dissipation in vibration control. Kurdila et al. [5] proved that this state-switching strategy reduces the energy of the system and is stable, and Ramaratnam and Jalili [6] implemented this idea of "switched stiffness" in vibration control experiments. In contrast to these results, where the purpose of stiffness variation is to dissipate energy, the authors [1,2] proposed stiffness variation for modal energy redistribution which then can be used for energy absorption, harvesting, or dissipation. Modal energy redistribution, which has also been observed in systems with

*Corresponding author. Tel.: +1 517 355 1834; fax: +1 517 353 1750.
E-mail address: mukherji@egr.msu.edu (R. Mukherjee).

0022-460X/$ - see front matter © 2007 Elsevier Ltd. All rights reserved.
doi:10.1016/j.jsv.2007.10.038

nonlinearities [7,8], should be differentiated from earlier work on localization [9–11], and energy pumping [12,13], where energy redistribution occurs spatially.

Stiffness variation and its effect on modal energy redistribution can be explained by means of a simple analogy where the amount of vibration energy present in a flexible structure is represented by a certain volume of fluid that needs to be drained away. A modal view corresponds to fluid (energy) that is distributed among a set of discrete containers, one for each mode. Fig. 1 depicts this situation using four modes, labeled A, B, C and D. In traditional modal control, the amount of fluid in each container has to be sensed separately and a controller that is capable of draining fluid from *all* the containers is used (Fig. 1a). Now consider a situation where the fluid in only one container, say container A (Fig. 1b), is sensed and then drained by a simple controller. Once all the fluid is removed from this container, the overall fluid volume decreases, but fluid remains trapped in the other containers, B, C, and D. Energy redistribution of the remaining fluid among all the containers, including moving some fluid into container A, can be achieved by stiffness variation. One step of stiffness variation, followed by draining of the fluid from container A, would leave fluid in the other containers, but repeating this process back and forth between two stiffness states will drain the fluid from all the containers.

The success of a stiffness variation approach to energy redistribution is measured by the total amount of energy that is transferred *into* a target mode (container A) at each step, and the details of how much energy is transferred *out* of the other modes, the source modes (containers B, C and D), at each step. The rate at which

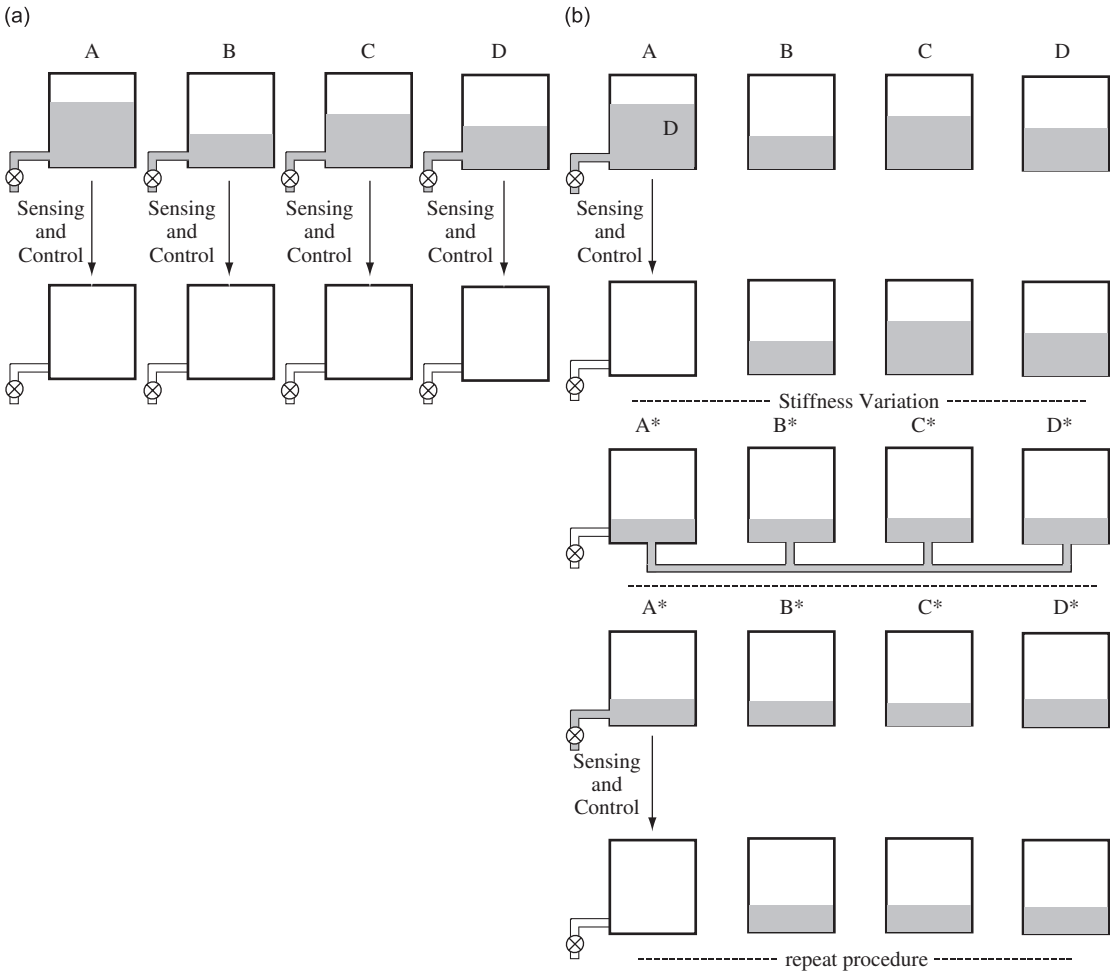

Fig. 1. A simple analogy to illustrate a control methodology based on the concept of modal disparity: (a) standard modal control strategy; (b) strategy based on stiffness variation.

energy is redistributed depends on the source modes. For instance, if a source mode in one stiffness state is nearly identical to a source mode in the other stiffness state (e.g., B and B* in Fig. 1b), then modal energy will drain very slowly from these modes, i.e., fluid will be essentially trapped in the corresponding containers. To quantify the amenability of a structure to energy redistribution strategies, a measure of energy redistribution is needed. *Modal disparity* is such measure. It is a property of the structure, as well as of the device introduced to effect the change in stiffness.

In the earlier work by the authors, [1,2], modal disparity of structures with variable stiffness were computed and simulation results of modal energy redistribution were provided. The objective of this paper is to experimentally demonstrate modal energy redistribution in a clamped–clamped beam with a variable stiffness joint. A mathematical model of the beam using finite elements is presented in Section 2. The mechanics of stiffness variation is discussed in Section 3. A modal coordinate description is provided in Section 4. Simulation results are presented in Section 5; they provide a benchmark for the experimental results presented in Section 6. Concluding remarks are provided in Section 7.

2. Finite element model

In this section we review the procedure to analyze the free vibration of a beam with a mid-span hinge, as shown in Fig. 2. The beam is clamped at both ends and the hinge can be locked or released to switch from one stiffness state to another. Assuming Euler–Bernoulli beam theory, the equation of motion of the beam in the x–y plane can be written as follows:

$$EIy'''' + m\ddot{y} = 0 \quad \text{if } x \in (0, L/2) \text{ or } x \in (L/2, L),$$

$$y(0,t) = y(L,t) = 0,$$

$$y'(0,t) = y'(L,t) = 0,$$

$$y((L/2)^-, t) = y((L/2)^+, t),$$

$$y'''((L/2)^-, t) = y'''((L/2)^+, t) \tag{1}$$

and in stiffness state α: hinge released

$$y''((L/2)^-, t) = 0,$$
$$y''((L/2)^+, t) = 0, \tag{2}$$

while in stiffness state β: hinge locked

$$y'((L/2)^-, t) = y'((L/2)^+, t),$$
$$y''((L/2)^-, t) = y''((L/2)^+, t). \tag{3}$$

In Eq. (1), E is the modulus of elasticity, I is area moment of inertia, and m is the mass per unit length of the beam.

The beam is modeled using N standard (cubic) finite elements, with two degrees of freedom per node (translation and rotation about the z-axis). To facilitate the modeling of the hinge in its two states, the node at $x = L/2$ has two rotational degrees of freedom, θ^l and θ^r, corresponding to $y'(L/2^-, t)$ and $y'(L/2^+, t)$, respectively. In stiffness state α, the hinge is assumed to be free and θ^l and θ^r are independent. However, in

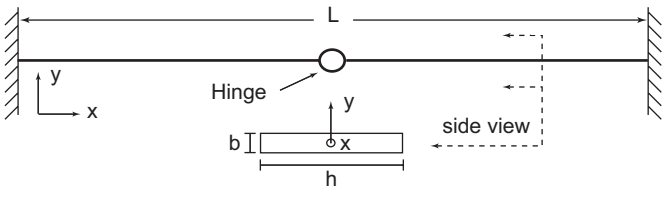

Fig. 2. A flexible clamped–clamped beam hinged in the middle.

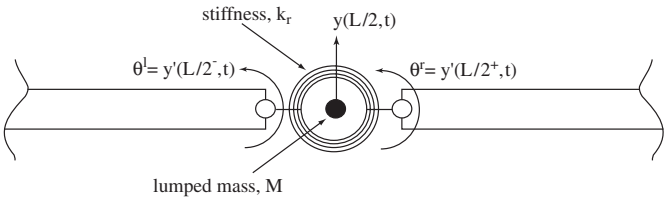

Fig. 3. The hinge model.

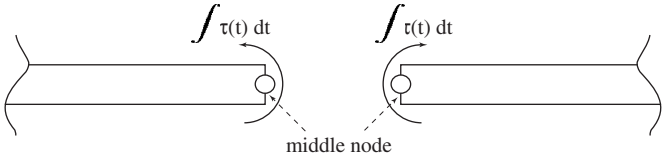

Fig. 4. Action–reaction pair of impulsive moments.

stiffness state β, the hinge is locked and the constraint $\theta^l = \theta^r$ has to be enforced. This is accomplished by adding a penalty of magnitude $\frac{1}{2}k_r(\theta^l - \theta^r)^2$ to the strain energy, that is, by adding a rotational stiffness

$$K_r = k_r \begin{bmatrix} 1 & -1 \\ -1 & 1 \end{bmatrix}, \tag{4}$$

to the global stiffness matrix. The parameter k_r is set to zero in the stiffness state α and to a large, positive value in stiffness state β. With the additional degree of freedom (in rotation) for the node at $x = L/2$, the finite element model has $(2N - 1)$ degrees of freedom.

The model of the hinge is shown schematically in Fig. 3. A lumped mass M is added at the central node to account for the mass of the hinge and the electromagnetic brake.

3. Mechanics of stiffness variation using a brake

The transition from stiffness state α to stiffness state β is achieved by activating an electromagnetic brake. The activation of the brake occurs over a brief interval of time and results in the application of an action-reaction pair of impulsive moments to the middle node, as shown in Fig. 4. If $t \in [t_{\alpha\beta}^-, t_{\alpha\beta}^+]$ denotes the activation time, the effect of the impulsive moments can be mathematically described by the relations

$$Y(t_{\alpha\beta}^-) = Y(t_{\alpha\beta}^+),$$

$$M\dot{Y}(t_{\alpha\beta}^-) + I_{\alpha\to\beta} = M\dot{Y}(t_{\alpha\beta}^+), \tag{5}$$

where M is the mass matrix and Y is the vector of nodal degrees of freedom. $I_{\alpha\to\beta}$ is the impulse vector with nonzero entries corresponding to the coordinates θ^l and θ^r and has the form

$$I_{\alpha\to\beta} = [0, \ldots, C, -C, \ldots, 0]^{\mathrm{T}}, \quad C = \int_{t_{\alpha\beta}^-}^{t_{\alpha\beta}^+} \tau(t)\,\mathrm{d}t, \tag{6}$$

where C is the impulse and τ is the impulsive moment. The displacements and velocities in stiffness state β right after activation of the brake, $Y(t_{\alpha\beta}^+)$ and $\dot{Y}(t_{\alpha\beta}^+)$, are calculated from the values of $Y(t_{\alpha\beta}^-)$ and $\dot{Y}(t_{\alpha\beta}^-)$ using Eq. (5). Although C is initially unknown, Eq. (5) can be solved without a problem since two elements of $\dot{Y}(t_{\alpha\beta}^+)$, namely $\dot{\theta}^l$ and $\dot{\theta}^r$, are equal.

The transition from stiffness state β to stiffness state α is achieved by releasing the brake. If $t \in [t_{\beta\alpha}^-, t_{\beta\alpha}^+]$ denotes the brief time interval over which the brake is released, the degrees of freedom and their velocities just

prior to and after release of the brake are the same, i.e.

$$Y(t_{\beta\alpha}^-) = Y(t_{\beta\alpha}^+), \quad \dot{Y}(t_{\beta\alpha}^-) = \dot{Y}(t_{\beta\alpha}^+). \tag{7}$$

Eqs. (5) and (7) describe the behavior of the system during the time intervals $t \in [t_{\alpha\beta}^-, t_{\alpha\beta}^+]$ and $t \in [t_{\beta\alpha}^-, t_{\beta\alpha}^+]$. At all other times, the beam behaves as a clamped–clamped beam with a frictionless hinge at mid-span (stiffness state α) or a clamped–clamped beam (stiffness state β). With this notation, the stiffness parameter k_r which was introduced in Section 2 is zero when in stiffness state α and when in stiffness state β is some large positive number k_∞ chosen to enforce the constraint $\theta^l = \theta^r$.

4. Modal coordinate description

Let ϕ_i and ψ_i denote the ith normalized mode shapes of the beam in stiffness state α and stiffness state β, respectively, and let $\mu_i(t)$ and $v_i(t)$ denote the corresponding modal displacements. In the two stiffness states, the vector of nodal degrees of freedom can be expressed as

$$Y(t) = \begin{cases} \sum_{i=1}^{2N-1} \mu_i(t)\phi_i & \text{stiffness state } \alpha, \\ \sum_{i=1}^{2N-1} v_i(t)\psi_i & \text{stiffness state } \beta. \end{cases} \tag{8}$$

The transition from stiffness state α to stiffness state β, mathematically described by Eq. (5), can now be rewritten as

$$\sum_{i=1}^{2N-1} \mu_i(t_{\alpha\beta}^-)\phi_i = \sum_{i=1}^{2N-1} v_i(t_{\alpha\beta}^+)\psi_i,$$

$$M \sum_{i=1}^{2N-1} \dot{\mu}_i(t_{\alpha\beta}^-)\phi_i + I_{\alpha\to\beta} = M \sum_{i=1}^{2N-1} \dot{v}_i(t_{\alpha\beta}^+)\psi_i. \tag{9}$$

Using Eq. (9), the modal displacements and velocities, $v_j(t_{\alpha\beta}^+)$ and $\dot{v}_j(t_{\alpha\beta}^+)$, can be expressed in terms of $\mu_j(t_{\alpha\beta}^-)$ and $\dot{\mu}_j(t_{\alpha\beta}^-)$ as follows:

$$v_j(t_{\alpha\beta}^+) = \sum_{i=1}^{2N-1} \psi_j^{\mathrm{T}} M\phi_i \mu_i(t_{\alpha\beta}^-),$$

$$\dot{v}_j(t_{\alpha\beta}^+) = \sum_{i=1}^{2N-1} \psi_j^{\mathrm{T}} M\phi_i \dot{\mu}_i(t_{\alpha\beta}^-). \tag{10}$$

In the derivation of Eq. (10) from Eq. (9), we used the identity $\psi_j^{\mathrm{T}} I_{\alpha\to\beta} = 0$. This is true since the entries of ψ_j, $j = 1, 2, \ldots (2N-1)$, corresponding to the nonzero entries of $I_{\alpha\to\beta}$, namely θ^l and θ^r, are equal.

Using the same procedure as above, the transition from stiffness state β to stiffness state α can be obtained from Eq. (7) as follows:

$$\mu_j(t_{\beta\alpha}^+) = \sum_{i=1}^{2N-1} \phi_j^{\mathrm{T}} M\psi_i v_i(t_{\beta\alpha}^-),$$

$$\dot{\mu}_j(t_{\beta\alpha}^+) = \sum_{i=1}^{2N-1} \phi_j^{\mathrm{T}} M\psi_i \dot{v}_i(t_{\beta\alpha}^-). \tag{11}$$

If we define $\Phi = [\phi_1, \phi_2, \ldots, \phi_{(2N-1)}]$ and $\Psi = [\psi_1, \psi_2, \ldots, \psi_{(2N-1)}]$, it is clear from Eqs. (10) and (11) that elements of the matrix $\Psi^{\mathrm{T}} M\Phi$ define the mapping between modal coordinates during the transition from stiffness state α to stiffness state β. The transposed matrix, $\Phi^{\mathrm{T}} M\Psi$, defines the mapping between modal coordinates during the transition from stiffness state β to stiffness state α. These matrices will be identity matrices if the two stiffness states are the same and any deviation from the identity structure is a measure of modal disparity between the two stiffness states [1].

5. Numerical example

Consider the clamped–clamped beam in Fig. 2 with the material and geometric properties in Table 1. The natural frequencies of the first four modes of the beam in the two stiffness states are shown in Table 2. Since the hinge is located at mid-span, the natural frequencies of even numbered modes in the two stiffness states are identical. This is true because even-numbered modes have zero curvature at mid-span and are not affected by the state of the hinge, i.e. locked or released. The first four mode shapes of the beam in the two stiffness states are provided in Fig. 5 for reference.

Using modal truncation, the matrix measure of modal disparity was computed using the first four modes as follows:

$$\Psi^{\mathrm{T}} M \Phi = \begin{pmatrix} 0.980 & 0.000 & 0.153 & 0.000 \\ 0.000 & 1.000 & 0.000 & 0.000 \\ 0.139 & 0.000 & 0.949 & 0.000 \\ 0.000 & 0.000 & 0.000 & 1.000 \end{pmatrix}. \tag{12}$$

Table 1
Material and geometric properties of clamped–clamped beam in Fig. 2

Material	Aluminum
Young's modulus	71 GPa
Density	2710 kg/m^3
Dimensions	$2.0 \times 0.05 \times 0.0023$ m^3
Hinge mass	0.182 kg

Table 2
Natural frequencies of the finite element model of the beam in the two stiffness states

$\omega_{\alpha i}$, $\omega_{\beta i}$ (rad/s)		mode number, i			
		$i=1$	$i=2$	$i=3$	$i=4$
Stiffness state	α	1.29	8.34	9.52	27.0
	β	2.30	8.34	14.68	27.0

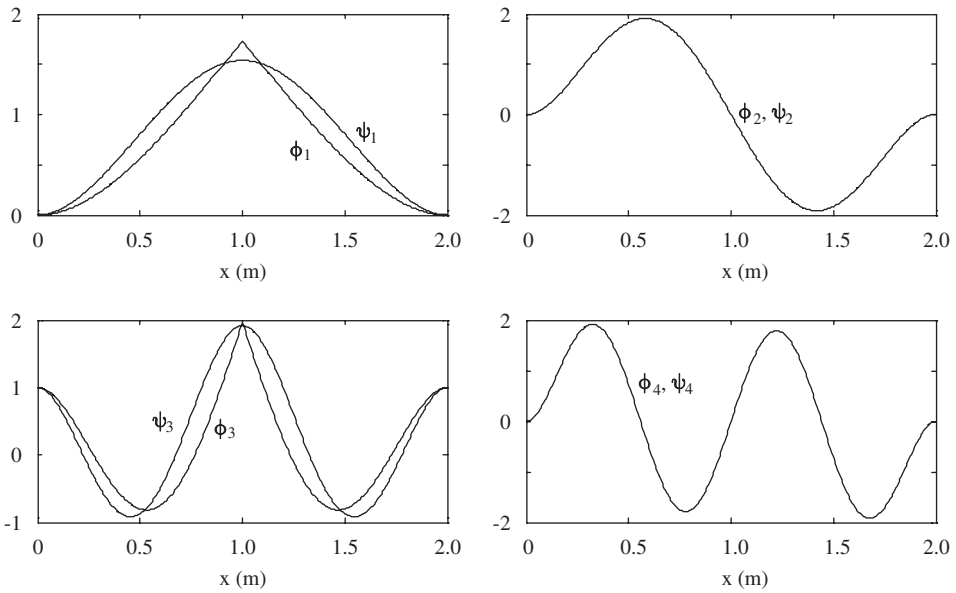

Fig. 5. Mode shapes of the clamped–clamped beam in the two stiffness states.

The second and fourth rows and columns of the matrix in Eq. (12) maintain the identity structure. This is indicative of the fact that even-numbered modes in the two stiffness states are identical. The nonzero elements in the off-diagonal entries of the matrix are indicative of the presence of modal disparity between the two stiffness states and indicate how modal energy will be redistributed between odd-numbered modes in these two states.

To illustrate modal energy redistribution between odd-numbered modes in the two stiffness states, we consider the scenario where the beam is initially in stiffness state α and vibrating purely in the third mode with an amplitude A. The total energy of the beam is equal to $E_\alpha = 0.5A^2\omega_{\alpha 3}^2$. It is assumed that there is no damping in the system and that the brake is activated when the beam passes through its neutral position. Since $\mu_i(t_{\alpha\beta}^-) = 0$, we have $v_i(t_{\alpha\beta}^+) = 0$ from Eq. (10). The modal velocities in stiffness states β can be computed from Eq. (10) as follows:

$$\begin{bmatrix} \dot{v}_1(t_{\alpha\beta}^+) \\ \dot{v}_2(t_{\alpha\beta}^+) \\ \dot{v}_3(t_{\alpha\beta}^+) \\ \dot{v}_4(t_{\alpha\beta}^+) \end{bmatrix} = \begin{pmatrix} 0.980 & 0.000 & 0.153 & 0.000 \\ 0.000 & 1.000 & 0.000 & 0.000 \\ 0.139 & 0.000 & 0.949 & 0.000 \\ 0.000 & 0.000 & 0.000 & 1.000 \end{pmatrix} \begin{bmatrix} 0 \\ 0 \\ A\omega_{\alpha 3} \\ 0 \end{bmatrix}. \tag{13}$$

Clearly, the energy of the beam is redistributed in modes 1 and 3 in stiffness state β. The amount of energy in these modes are:

$$E_{\beta 1} = \tfrac{1}{2}0.153^2 A^2\omega_{\alpha 3}^2 = 0.153^2 E_\alpha,$$

$$E_{\beta 2} = \tfrac{1}{2}0.949^2 A^2\omega_{\alpha 3}^2 = 0.949^2 E_\alpha. \tag{14}$$

It can be easily shown that the amplitudes of these modes are $0.153A(\omega_{\alpha 3}/\omega_{\beta 1}) = 0.633A$ and $0.949A(\omega_{\alpha 3}/\omega_{\beta 3}) = 0.615A$, respectively. These results will be validated through experiments in the next section.

6. Experimental verification

The experimental hardware is shown in Fig. 6. The beam has a pair of piezoelectric transducers[1] mounted on each side at a distance of 5 cm from one of the clamped ends. These transducers are used for excitation. A single piezoelectric strain sensor[2] is mounted on the beam at a distance of 5 cm from the other clamped end. The position of the sensor and actuators are chosen based on high degree of controllability and observability of the first three modes of the system. The material and geometric properties of the beam in the experimental setup are the same as those used in simulations and provided in Table 1. In this table, the hinge mass includes the mass of the electromagnetic brakes,[3] shown in Fig. 6, used for locking and releasing the hinge.

In our experiments, we chose to investigate energy redistribution between the first three modes of the beam. This was motivated by the fact that modal disparity can be adequately demonstrated by the first three modes and estimation of the higher modes are more prone to inaccuracies. The first three natural frequencies were experimentally determined for both stiffness states and are provided in Table 3. The piezoelectric transducers were used to excite the beam and the strain sensor was used to measure beam vibration. The natural frequencies were identified as the frequencies of excitation that resulted in maximal amplitude of vibration. The experimentally determined values show good agreement with the numerically computed values in Table 2.

We first present experimental results for two cases where the beam was initially in stiffness state α (hinge released) and switched to stiffness state β (hinge locked). For the first case, Case A, the beam was excited at its second natural frequency in stiffness state α. The stiffness of the beam was switched after termination of excitation and the results, shown in Fig. 7, indicate that the beam vibrates primarily in its second mode in stiffness state β. This is expected since the second mode of the two stiffness states are identical.

[1]Product of Mide Technology Corporation.
[2]Product of PCB Piezotronics.
[3]Product of Inertia Dynamics.

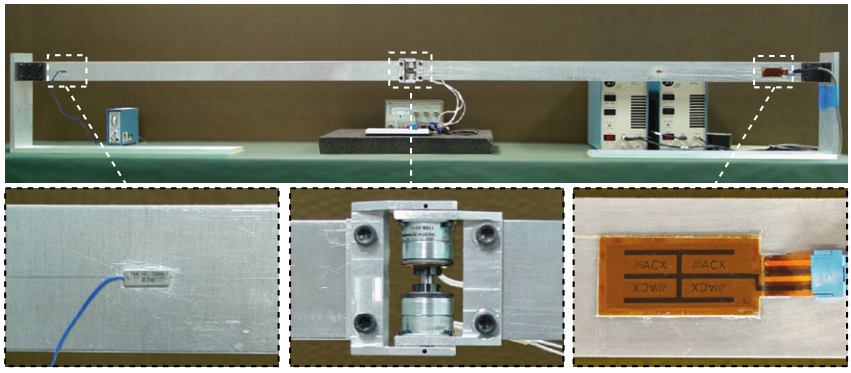

Fig. 6. Experimental hardware.

Table 3
Natural frequencies of the beam in the two stiffness states, determined experimentally

$\omega_{\alpha i}$, $\omega_{\beta i}$ (rad/s)		mode number, i		
		$i=1$	$i=2$	$i=3$
Stiffness state	α	1.40	8.24	9.70
	β	2.37	8.20	13.90

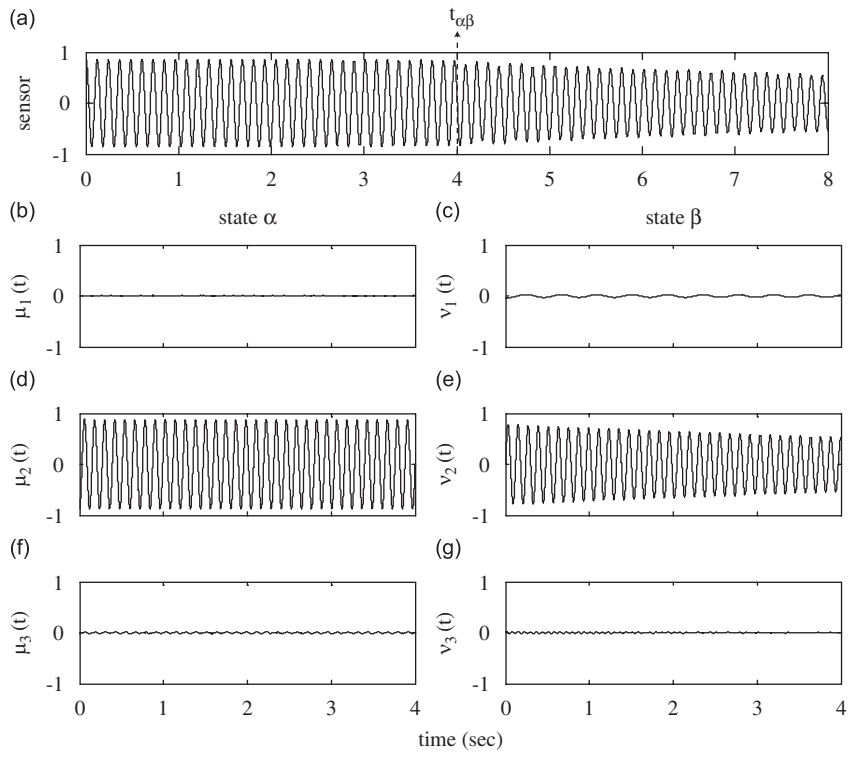

Fig. 7. Energy redistribution between modes for Case A: (a) sensor output; (b), (d) and (f) modal amplitudes in state α. (c), (e) and (g) modal amplitudes in state β.

This can be verified from the elements of the second column vector of the modal disparity matrix $\Psi^{T}M\Phi$ in Eq. (12). All entries of this vector are zero except for the second entry, which is unity.

For the second case, Case B, the beam was excited at its third natural frequency in stiffness state α. Its stiffness was switched after termination of excitation and the results are shown in Fig. 8. Since the first and third elements of the third column vector of $\Psi^{T}M\Phi$ are nonzero, the beam vibrates in its first and third natural frequencies in stiffness state β. The amplitude of these modes, immediately after the switch, can be computed based on our analysis in the last section. These values and the values obtained from experiments are both presented in Table 4 and they show good conformity. The plots in Fig. 8 indicate a small presence of the second mode in both stiffness states. It is logical to infer that excitation of the beam introduced the second mode in stiffness state α and energy associated with this mode transferred directly to the second mode in stiffness state β.

For the sake of completeness, we present experimental results for one case where the beam was initially in stiffness state β (hinge locked) and switched to stiffness state α (hinge released). The results for this case, which

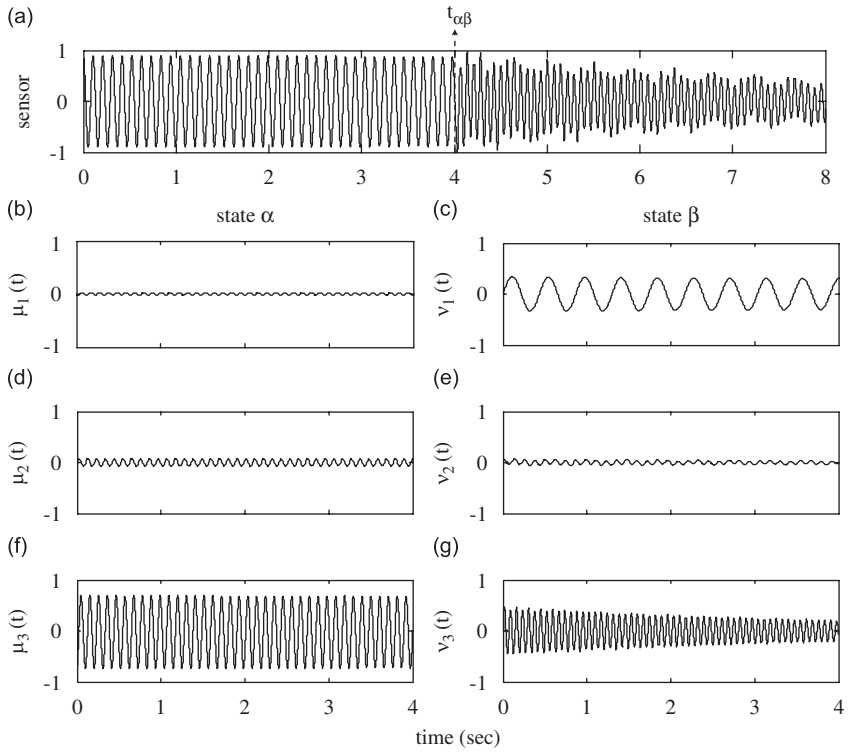

Fig. 8. Energy redistribution between modes for Case B: (a) sensor output; (b), (d) and (f) modal amplitudes in state α; (c), (e) and (g) modal amplitudes in state β.

Table 4
Modal amplitudes immediately before and after switchings

	Stiffness switch	Amplitudes before switch Mode number i			Amplitudes after switch Actual/expected values		
		$i=1$	$i=2$	$i=3$	$i=1$	$i=2$	$i=3$
Case A	$\alpha \to \beta$	0.01	0.88	0.01	0.02/0.01	0.80/0.88	0.01/0.01
Case B	$\alpha \to \beta$	0.02	0.07	0.68	0.36/0.42	0.05/0.07	0.44/0.45
Case C	$\beta \to \alpha$	0.00	0.84	0.01	0.01/0.00	0.79/0.84	xxx/0.00

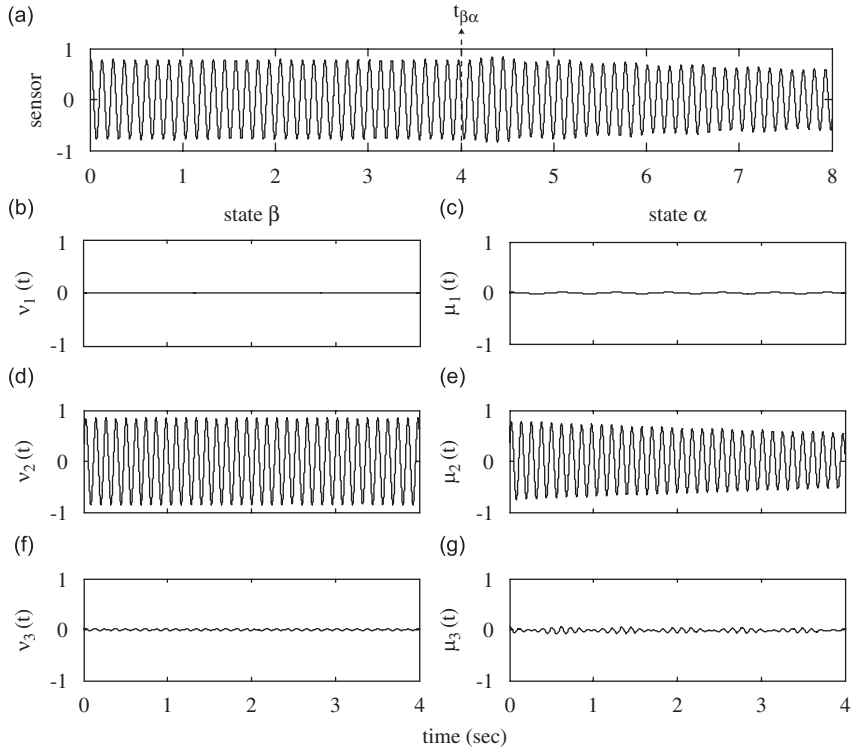

Fig. 9. Energy redistribution between modes for Case C: (a) sensor output; (b), (d) and (f) modal amplitudes in state β; (c), (e) and (g) modal amplitudes in state α.

we denote as Case C, are shown in Fig. 9 and summarized in Table 4. For this case, the beam vibrates in its second mode in stiffness state β and energy associated with this mode is entirely transferred to the second mode in stiffness state α, upon switching. The results for this case are therefore quite similar to that of Case A. The amplitude of the third mode in stiffness state α could not be measured accurately and is marked "xxx" in Table 4. The difficulty of the measurement was due to its small magnitude coupled with waxing and waning due to beating. The beating phenomenon can be attributed to the close proximity of the second and third natural frequencies of the beam in stiffness state α.

7. Conclusion

This investigation has confirmed that changes in structural stiffness result in modal disparity, and that this disparity permits energy to be transferred between different sets of spatial modes in a given structure. Finite element based analysis and systematic experiments have demonstrated that the phenomena can be modeled and quantitatively predicted. One of the keys in the modeling is to properly account for the physics of the transition between the different stiffness states, which results in the correct mapping of the modal energies from one set of modes to another. With these tools in hand, it should be possible to design structural systems with built-in mechanisms for stiffness variation for favorable modal disparity, and to predict the efficacy of various proposed switching schemes. Our earlier work [1,2], explored efficient means for funneling energy in a vibrating structure to a select set of target modes with the underlying objective of reducing the total number of sensors and actuators required for vibration control. A topology optimization problem was solved to determine the "best locations" for stiffness change for a predefined set of target modes but the problem can be easily redefined to determine the target modes for a predefined change in stiffness. Our future studies will include: transition between multiple stiffness states, or even continually-varying stiffness states; the integration of modal disparity with structural control, active or passive, wherein one controls only a subset of modes in

each set, and the repeated exchange of modal energies permits the ultimate dissipation of energy in all the modes; the use of stiffness changes that are timed in a particular manner so as to inherently dissipate energy in the system; the implementation of stiffness variation to generate modal disparity in more complex structures, including plane and space frames and trusses; and various combinations of the above-listed ideas.

Acknowledgments

The authors gratefully acknowledge the support provided by Air Force Office of Scientific Research, AFOSR Grant FA9550-04-1-0069, for this work.

References

[1] A.R. Diaz, R. Mukherjee, Modal disparity enhancement through optimal insertion of non-structural masses, *Structural and Multidisciplinary Optimization* 31 (1) (2006) 1–7.
[2] A.R. Diaz, R. Mukherjee, A topology optimization problem in control of structures using modal disparity, *ASME Journal of Mechanical Design* 128 (2006) 536–541.
[3] W.W. Clark, Vibration control with state-switching piezoelectric materials, *Journal of Intelligent Material Systems and Structures* 11 (4) (2000) 263–271.
[4] L.R. Corr, W.W. Clark, Energy dissipation analysis of piezoceramic semiactive vibration control, *Journal of Intelligent Material Systems and Structures* 12 (2001) 729–736.
[5] A.J. Kurdila, W.W. Clark, W. Wang, D.E. MacDaniel, Stability of a class of piezoelectric state-switching methods, *ASME International Mechanical Engineering Congress and Exposition*: *Adaptive Structures and Material Systems*, Orlando, FL, AD-60, November 2000, pp. 477–484.
[6] A. Ramaratnam, N. Jalili, A switched stiffness approach for structural vibration control: theory and real-time implementation, *Journal of Sound and Vibration* 291 (2006) 258–274.
[7] P. Malatkar, A.H. Nayfeh, On the transfer of energy between widely spaced modes in structures, *Nonlinear Dynamics* 31 (2) (2003) 225–242.
[8] J.P. Cusumano, F.C. Moon, Chaotic non-planar vibrations of the thin elastica. Part 1: experimental observation of planar instability, *Journal of Sound and Vibration* 179 (2) (1995) 185–208.
[9] C.H. Hodges, Confinement of vibration by structural irregularity, *Journal of Sound and Vibration* 82 (1982) 411–424.
[10] C. Pierre, E.H. Dowell, Localization of vibration by structural irregularity, *Journal of Sound and Vibration* 114 (1987) 549–564.
[11] A.F. Vakakis, T.K. Centikaya, Mode localization in a class of multi-degree of freedom systems with cyclic symmetry, *SIAM Journal on Applied Mathematics* 53 (1993) 265–282.
[12] G. Kerschen, Y.S. Lee, A.F. Vakakis, D.M. MacFarland, L.A. Bergman, Irreversible passive energy transfer in coupled oscillators with essential nonlinearity, *SIAM Journal on Applied Mathematics* 66 (2) (2006) 648–679.
[13] A.F. Vakakis, Designing a linear structure with a local nonlinear attachment for enhanced energy pumping, *Mechanica* 38 (2003) 677–686.